Electrodeposition of Al-W alloy films in a 1-ethyl-3-methyl-imidazolium chloride-AlCl ionic liquid containing WCl

Higashino, Shota; Miyake, Masao; Fujii, Hisashi; Takahashi, Ayumu; Hirato, Tetuji

Electrodeposition of Al-W Alloy Films in a 1-Ethyl-3-methyl-imidazolium Chloride-$AlCl_3$ Ionic Liquid Containing W_6Cl_{12}

Shota Higashino, Masao Miyake,[z] Hisashi Fujii, Ayumu Takahashi, and Tetuji Hirato*

Graduate School of Energy Science, Kyoto University, Yoshida-honmachi, Sakyo-ku, Kyoto 606-8501, Japan

The electrodeposition of Al-W alloy films in a Lewis acidic 1-ethyl-3-methyl-imidazolium chloride (EMIC)-$AlCl_3$ ionic liquid using W_6Cl_{12} as the W ion source was investigated. W_6Cl_{12} dissolved in the ionic liquid at a higher concentration than other W ion sources used in previous studies. Potentiostatic electrodeposition was performed in a bath containing W_6Cl_{12} at a concentration of 49 mM. Dense Al-W alloy films containing up to 12 at.% W were electrodeposited at potentials more negative than 0 V vs. Al/Al(III). The deposition current density at >0 V was lower than 0.3 mA cm^{-2}, while that for Al-W alloy films was higher and reached 38 mA cm^{-2} at −0.5 V. The deposition of W was induced by the deposition of Al. At lower W concentrations, the Al-W alloy films were composed of a super-saturated solid solution, and in the W content range of 9–12 at.% they comprised an amorphous phase. Potentiodynamic polarization and nano-indentation showed that the Al-W alloy films containing 10–12 at.% W exhibited high pitting corrosion resistance, high hardness, and low Young's modulus.

Manuscript submitted October 27, 2016; revised manuscript received January 4, 2017. Published January 21, 2017.

Al metal has high oxidation and corrosion resistance, and its chloride-induced pitting corrosion resistance is enhanced by alloying with transition metals. Consequently, Al-transition metal alloys have attracted much research attention as corrosion-protective materials. Among these alloys, Al-W alloys containing approximately 10 at.% are known to exhibit the greatest resistance to pitting corrosion.[1]

Since the maximum solubility of W in Al phases is only 0.022 at.% at 640°C in the equilibrium state,[2] the formation of Al-W alloy films having high corrosion resistances requires non-equilibrium processes, such as sputtering,[1,3–8] ion implantation,[9] and electrodeposition.[10–12] Of these methods, electrodeposition has particular advantages in that a uniform film can be formed relatively quickly and continuously, onto substrates having complex shapes, using simple equipment. Various Al-based alloy films have been electrodeposited in molten salts such as NaCl-$AlCl_3$ with the addition of ion sources for the alloy component. Recently, electrodeposition using ionic liquids has become more popular owing to their low melting point and low volatility. A representative ionic liquid used for the electrodeposition of Al alloys is Lewis acidic 1-ethyl-3-methylimidazolium chloride (EMIC)-$AlCl_3$ (where the $AlCl_3$/EMIC molar ratio >1). Reports on the electrodeposition of Al alloys including Al-Ni,[13] Al-Ti,[14] Al-V,[15] Al-Zr,[16] Al-Mo,[17] Al-Mn,[18] and Al-Hf[19] are available in the literature.

A previous study revealed that electrodeposition in a EMIC-$AlCl_3$ bath with the addition of W(IV) chloride (WCl_4) yielded Al-W alloys, but the W content was lower than 1 at.%.[10] Recently, the electrodeposition of Al-W alloy films from an EMIC-$AlCl_3$ bath with the addition of the W(III) compound $K_3W_2Cl_9$ was reported.[11,12] Although the W content of the Al-W alloys reached nearly 96 at.%, the deposits with high W content had powdery morphologies. When the current density was high (>20 mA cm^{-2}), dense Al-W alloy films were obtained, but the W content decreased to <3 at.%. This decrease in the W content at high current density was due to the rate of W deposition into the alloy film being controlled by the diffusion of W ions in the bath. The diffusion-controlled deposition of W was inevitable in this liquid because it was saturated with $K_3W_2Cl_9$ at concentrations as low as 8 mM at 80°C.

To electrodeposit dense Al-W alloy films with a high W content at a high current density, an effective approach is to use a W ion source that can dissolve in EMIC-$AlCl_3$ at high concentration. Consequently, we have focused on W_6Cl_{12} as the W ion source. Our preliminary experiments revealed that the solubility of W_6Cl_{12} in EMIC-$AlCl_3$ is significantly higher than that of $K_3W_2Cl_9$. In addition, the oxidation number of W is lower in W_6Cl_{12} (i.e., II) than in $K_3W_2Cl_9$ (i.e., III), and therefore we expected that W_6Cl_{12} would reduce more easily to metallic W. In this study, electrodeposition in EMIC-$AlCl_3$ containing W_6Cl_{12} was examined. The W content, surface morphology, and crystal structure of the resulting deposits were investigated. Furthermore, the pitting corrosion resistance and mechanical properties of the dense Al-W alloy films with high W contents of approximately 10–12 at.% were evaluated.

Experimental

Preparation of the electrolytic bath.—The electrolytic bath was prepared by adding anhydrous aluminum chloride ($AlCl_3$, 99%, Fluka) to EMIC (97%, Tokyo Chemical Industry) at a molar ratio of 2:1. The EMIC was dried under vacuum at 120°C prior to use. The W ion source, W_6Cl_{12}, was synthesized by a method similar to those described in previous reports.[20,21] Briefly, a mixture of tungsten(VI) chloride (WCl_6, 99.9%, Wako) and bismuth powder (Bi, 99.9%, Wako) at a molar ratio of 3:4 was charged into a two-chamber glass tube and flame-sealed under vacuum. The mixture placed in one chamber was heated in a furnace, first at 280°C for 2 days and then at 355°C for more than 5 days. During the heating at 355°C, WCl_6 was reduced by Bi to produce W_6Cl_{12}, and the by-product, $BiCl_3$, was sublimed into the other chamber, which was exposed to a lower temperature. After heating, black powder collected from the product chamber was washed with concentrated aqueous HCl at room temperature, and then dissolved in boiling concentrated aqueous HCl. From the solution, yellow crystals of $(H_3O)_2[W_6Cl_{14}]\cdot 7H_2O$ were recrystallized. The crystals of $(H_3O)_2[W_6Cl_{14}]\cdot 7H_2O$ were heated at 325°C for 1 h in vacuum, yielding a bright yellow powder of W_6Cl_{12}. EDX confirmed that the Cl/W atomic ratio of the powder was 2. XRD patterns of the powder agreed with that of poorly crystallized W_6Cl_{12}.[22] The synthesized W_6Cl_{12} powder was added to the EMIC-2$AlCl_3$ bath until it was saturated.

Electrochemical experiments.—Electrochemical experiments using the EMIC-2$AlCl_3$-W_6Cl_{12} bath were carried out in an argon-filled glove box (SDB-1AO, MIWA MFG). A glass vessel with a volume of 25 mL was used as an electrolytic cell. The bath temperature was kept at 80°C by a heater and thermostat (TJA-550, AS ONE) connected to a rubber heater wound around the cell and a thermocouple soaked in the

*Electrochemical Society Member.
[z]E-mail: miyake.masao.4e@kyoto-u.ac.jp

bath. Cyclic voltammograms were recorded using a Pt electrode and an Al plate as the working and counter electrodes, respectively. An Al wire immersed in neat EMIC-2$AlCl_3$ ionic liquid separated from the bath by a porous glass frit (BAS) was used as the reference electrode. The potential scan was started from the open circuit potential to the cathodic direction at a sweep rate of 10 mV s^{-1}.

Potentiostatic electrodeposition was performed on a mirror polished Cu plate. A section of the Cu plate was covered with PTFE tape so that a certain area (5 mm × 5 mm) would be exposed. An Al plate and the aforementioned Al wire electrode were used as the counter and reference electrodes, respectively. The Cu plate and Al plate were placed vertically and in parallel with each other. The distance between the Cu and Al plates was less than 10 mm. During the electrodeposition process, the bath was agitated at 150 rpm using a magnetic stirrer (PC-420D, CORNING) and a magnetic flea (15 mm × 5 mm). The electrochemical experiments described above were carried out using an electrochemical analyzer (660c, ALS). After electrodeposition, the deposit was washed with distilled water and ethanol.

Characterization of the deposit.—A scanning electron microscope (SEM, S-3500, Hitachi) combined with energy dispersive X-ray spectroscopy (EDX, INCAxact, Oxford Instruments) was used to observe the morphology and measure the elemental composition of the deposit. X-ray diffraction (XRD) patterns were obtained using an X-ray diffractometer (X'pertPRO-MPD, PANalytical) with Cu-Kα radiation. Some of the deposits were analyzed with X-ray photoelectron spectrometry (XPS; JPS-9010TRX, Nihon Denshi). The partial current density for the deposition of W was calculated from the amount of deposited W, as determined by inductively coupled plasma-atomic emission spectroscopy (ICP-AES; Optima 5300 DV, PerkinElmer). The sample solution for the ICP-AES was prepared by dissolving the deposit in 5 mM aqueous NaOH solution. To promote the dissolution of W, a small amount of H_2O_2 solution was added to the solution. After the deposit was completely dissolved, residual H_2O_2 was vaporized by heating the solution to 70°C. The pitting corrosion resistance of an Al plate (99.5%, Nilaco) and the Al-W alloy films was evaluated from potentiodynamic polarization curves in 3.5 wt% aqueous NaCl solution, which was deaerated with bubbling argon gas prior to each experiment. A Pt plate and an Ag/AgCl/sat. KCl electrode were used as the counter and reference electrodes, respectively. The potential scan was started from −0.8 V in the anodic direction at a sweep rate of 0.5 mV s^{-1}. The potential scan was performed using an electrochemical analyzer (HZ-5000, Hokuto Denko). The hardnesses and Young's moduli of the Al-W alloy films were determined by nanoindentation tests using an nano-indenter (G200, Agilent Technologies) with a diamond Berkovich tip. The surface of the electrodeposited 10-μm thick Al and Al-W alloy films was mirror polished prior to the indentation tests. Indentation data was collected using the continuous stiffness measurement (CSM) technique with a vibration frequency of 45 Hz. In each indentation, the hardness and Young's modulus value were obtained at a depth of 1 μm, where no significant effect of the substrate material was seen. The values reported for the hardnesses and Young's moduli are averages of the values taken at 12 indentation points, which were separated by more than 50 μm in all directions. In the evaluation of the Young's moduli, the Poisson's ratio of the Al-W alloy films was assumed to be 0.3.

Results and Discussion

Solubility of W_6Cl_{12} in EMIC-2$AlCl_3$.—W_6Cl_{12} was added to the Lewis acidic EMIC-2$AlCl_3$ until it was saturated. The saturation concentration of W_6Cl_{12} was 49 mM at 80°C. W_6Cl_{12} and Mo_6Cl_{12} have the same atomic arrangement in their crystal structures, which both comprise a $[M_6Cl_8]^{4+}$ core, where M = W or Mo.[23,24] Mo_6Cl_{12} is believed to dissolve in EMIC-2$AlCl_3$ while maintaining the form of the $[Mo_6Cl_8]^{4+}$ core in solution.[25] W_6Cl_{12} should also dissolve in EMIC-2$AlCl_3$ in the same manner as Mo_6Cl_{12} by the following reaction:

$$x\ Al_2Cl_7^- + W_6Cl_{12} \leftrightarrow 2x\ AlCl_4^- + [W_6Cl_8]Cl_{4-x}^{x+} \quad [1]$$

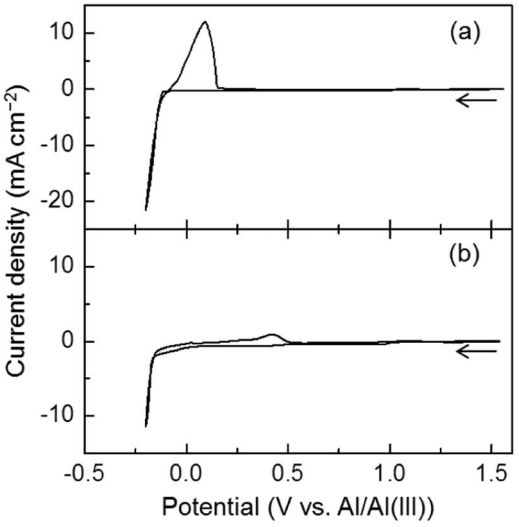

Figure 1. Cyclic voltammograms recorded at a Pt electrode in an EMIC-2$AlCl_3$ bath at 80°C (a) before and (b) after the addition of 49 mM W_6Cl_{12}. The scan rate was 10 mV s^{-1}.

Cyclic voltammetry.—Figure 1 shows cyclic voltammograms recorded at a Pt electrode in the EMIC-2$AlCl_3$ bath before and after the addition of 49 mM W_6Cl_{12}. Before the addition of W_6Cl_{12} (Fig. 1a), the cathodic current rises steeply at −0.1 V during the cathodic scan. After the scan is reversed at −0.2 V, an anodic current with a peak at +0.1 V is observed. These cathodic and anodic currents are due to the deposition and stripping, respectively, of Al. After the addition of 49 mM W_6Cl_{12} (Fig. 1b), a small cathodic current is observed in the potential range from +0.4 V to −0.15 V, and the cathodic current rises steeply at −0.15 V. After the scan is reversed, a small anodic current is observed with a peak at +0.4 V. The small cathodic current in the potential range from +0.4 V to −0.15 V is not observed before the addition of W_6Cl_{12}. Therefore, there is a possibility that this cathodic current is caused by the reduction of W ions. The shift in the anodic current peak to a more positive potential upon the addition of W_6Cl_{12} indicates that an Al-W alloy phase is formed during the cathodic scan. By alloying with W, which is more noble than Al, Al becomes more difficult to dissolve during the anodic scan.

Potentiostatic electrodeposition and characterization of the deposits.—Potentiostatic electrodeposition was carried out at every 0.1 V in the potential range from −0.5 to +0.4 V vs. Al/Al(III). The amount of charge was set at 8.0 C cm^{-2}, which corresponds to the value required to electrodeposit a 2.8-μm thick pure Al film or a 3.9-μm thick pure W film, assuming 100% current efficiency.

The steady-state cathodic current density is as low as 0.3 mA cm^{-2} at potentials more positive than 0 V. In contrast, at potentials more negative than 0 V, the current density increases with decreasing potential, and reaches 38 mA cm^{-2} at −0.5 V.

Every electrodeposition in the potential range from −0.5 V to +0.4 V yields deposits on the Cu cathode substrates. The appearance of the deposit varies significantly at a potential of 0 V. In the potential range from 0 to +0.4 V, the deposits are black, and exhibit poor adhesion to the substrates. In the potential range from −0.5 to −0.1 V, the deposits are gray, and exhibit good adherence. The typical EDX spectra of the deposits obtained at potentials: >0 V and <0 V, are shown in Fig. 2. EDX shows that all these deposits contain Al and W. The presence of other elements such as Cu and O is also observed, owing to substrate and surface oxidation, respectively. The larger signals of Cu and O from the deposits obtained at potentials

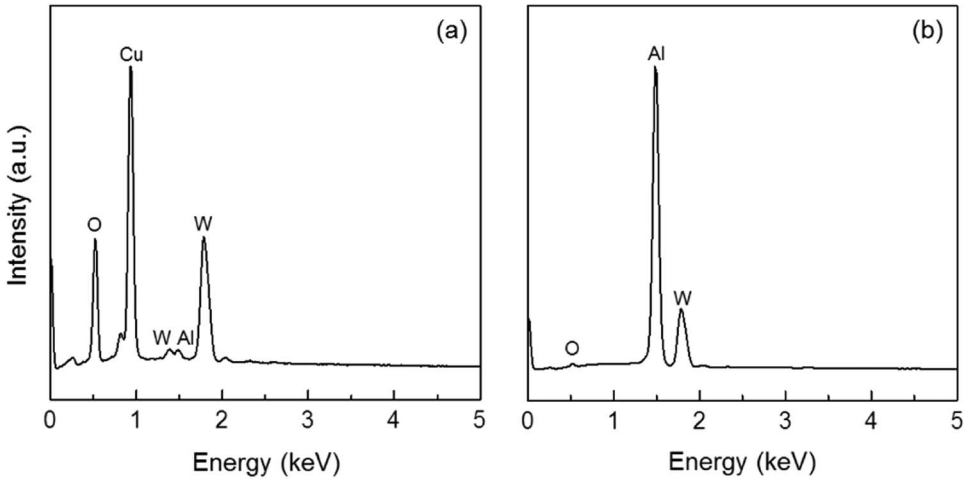

Figure 2. Typical EDX spectra of the deposits obtained from an EMIC-2AlCl$_3$ bath containing 49 mM W_6Cl_{12}. The applied potentials are: (a) +0.3 V and (b) −0.5 V.

>0 V are probably derived from the presence of many cracks in the deposits, as discussed in detail later. The W content calculated by only taking into account the presence of Al and W is plotted against the deposition potential, as shown in Fig. 3. The W content of the deposit also changes drastically across 0 V. In the potential range from 0 to +0.4 V, the W content is high (64–92 at.%) with a large scattering. In the potential range from −0.5 to −0.1 V, the W content is low (6.6–12 at.%), and has a small potential dependency.

Figure 4 shows the surface SEM images of the deposits. The deposit containing 64 at.% W obtained at +0.1 V (Fig. 4a) exhibits many cracks. The enlarged image reveals that some parts of the deposit are exfoliated from the substrate. This cracking and exfoliation is typical for deposits with high W contents electrodeposited at potentials more positive than 0 V. The deposit containing 6.6 at.% W obtained at −0.1 V (Fig. 4b) is composed of grains with leaf-like morphology. The deposits containing 9.1–11.8 at.% W electrodeposited at −0.2−0.5 V (Figs. 4c–4f) are composed of rounded and needle-like nodules with diameters less than 3 μm and no crystallographic facets. As shown by the arrow in the insets of Figs. 4d and 4e, some of the rounded nodules appear to have grown into those with needle-like shapes. The deposits at −0.2 −0.5 V (Figs. 4c–4f) form dense films with no cracks.

The XRD patterns of the deposits are shown in Fig. 5. The deposit obtained at +0.3 V presents no clear diffractions, except for those from the Cu substrate. All the deposits containing >64 at.% W obtained at potentials more positive than 0 V present no clear diffractions. This suggests that these deposits are amorphous, or not thick enough to cause detectable diffractions. In contrast, clear signals are detected from the deposits with up to 12 at.% W obtained at potentials more negative than 0 V. The deposit with 6.6 at.% W obtained at −0.1 V show a characteristic diffraction pattern for fcc Al. The deposits with 9.1–11.4 at.% W obtained at −0.2, −0.4, and −0.5 V also show the pattern for fcc Al, but the peak intensities are significantly smaller. In addition, a broad halo appears at around $2\theta = 42^\circ$. The deposit with 11.8 at.% W obtained at −0.3 V shows only a broad halo.

An enlarged view of the Al(111) diffraction peaks is shown in the right-hand graph in Fig. 5. The Al(111) peak positions of the deposits with 6.6–11.4 at.% W shift to higher angles compared to that of the electrodeposited Al metal. These peak shifts indicate the formation of

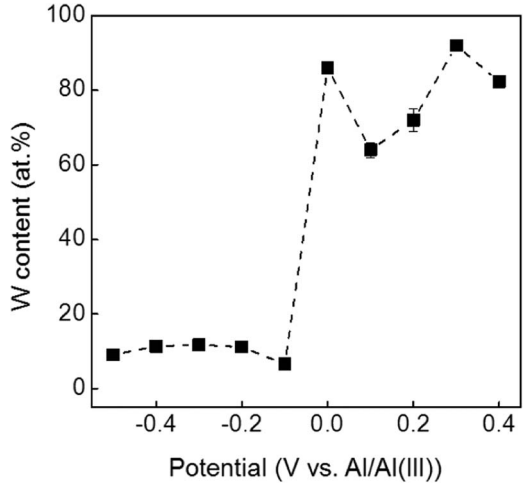

Figure 3. W content of the deposits obtained at various applied potentials in an EMIC-2AlCl$_3$ bath containing 49 mM W_6Cl_{12}.

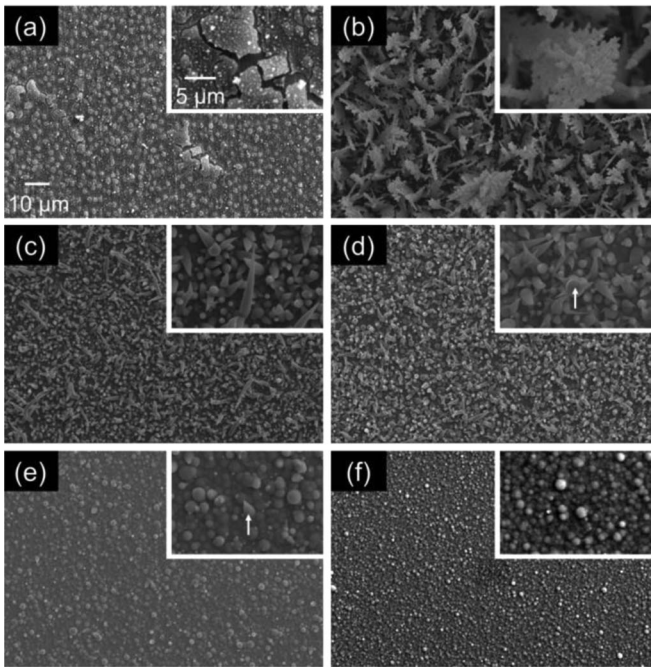

Figure 4. Surface SEM images of the deposits obtained in an EMIC-2AlCl$_3$ bath containing 49 mM W_6Cl_{12}. The applied potentials and the W contents of the deposits are; (a) +0.1 V, 64 at.%, (b) −0.1 V, 6.6 at.%, (c) −0.2 V, 11.2 at.%, (d) −0.3 V, 11.8 at.%, (e) −0.4 V, 11.4 at.%, (f) −0.5 V, 9.1 at.%.

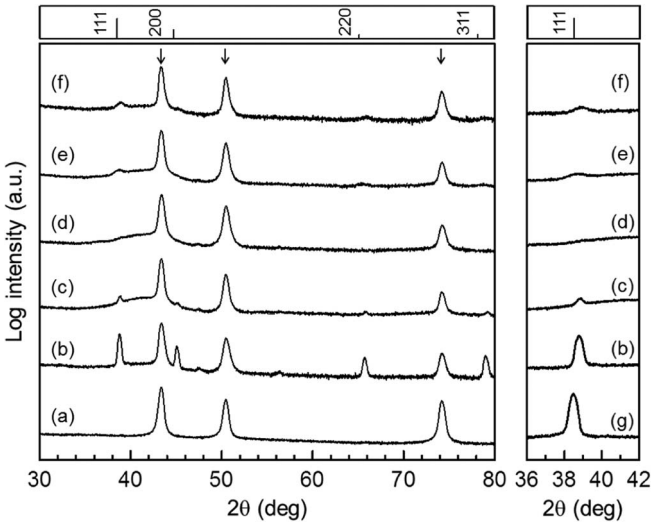

Figure 5. (Left) XRD patterns of the deposits obtained in an EMIC-2$AlCl_3$ bath containing 49 mM W_6Cl_{12}. The applied potentials and the W contents of the deposits are; (a) +0.3 V, 92 at.%, (b) −0.1 V, 6.6 at.%, (c) −0.2 V, 11.2 at.%, (d) −0.3 V, 11.8 at.%, (e) −0.4 V, 11.4 at.%, (f) −0.5 V, 9.1 at.%. The arrows indicate the diffraction peaks from the Cu substrate. The peak positions for fcc Al (ICDD: 00-004-0787) are shown at the top of the figure. (Right) An enlarged view of the Al(111) diffraction peaks of the deposits and (g) an electrodeposited Al film.

a solid solution of fcc Al containing W atoms, which have a smaller radius than the Al atoms. According to Al-W binary phase diagrams, the maximum solubility of W in fcc Al is 0.022 at.% at 640°C.[2] Therefore, a super-saturated Al-W solid solution constitutes the deposits with 6.6–11.4 at.% W. The deposit with 6.6 at.% W, which shows clear fcc Al diffractions, is mainly composed of a solid solution. In contrast, the deposits with 9.1–11.4 at.% W show weaker diffractions for fcc Al and a broad halo around $2\theta = 42°$, indicating that these deposits contain a small amount of the solid solution phase, and a large amount of an amorphous phase. The deposit with 11.8 at.% W shows only a halo around $2\theta = 42°$, indicating that this deposit is composed of an amorphous phase only. The presence of amorphous phase in the deposits with 9–12 at.% W is in agreement with the fact that the deposits are composed of nodules with no crystallographic facets (Figs. 4c–4f). The formation of the super-saturated solid solution and the amorphous phase was also observed in the electrodeposition of Al-W alloy in the bath containing $K_3W_2Cl_9$, although the amorphous phase appeared at a lower W content (5 at.%).[12]

The XRD analysis was not able to reveal the phase of the deposits with a high W content obtained at potentials more positive than 0 V, because the diffraction signals were too small. In these cases, the deposits were examined with XPS. Figure 6 shows the W 4f and Al 2s spectra of the deposit obtained at +0.3 V (92 at.% W) before and after Ar^+ etching. The peak seen at 122.5 eV in Fig. 6b is the Cu 3s peak derived from the substrate.[26] Before Ar^+ etching, the W 4f spectra (Fig. 6a) shows peaks ascribable to W_2O_5 and WO_3. The Al 2s spectra (Fig. 6b) show peaks for Al_2O_3. After Ar^+ etching for 30 s, the peak intensity for the W oxides in the W 4f spectra decreases, and peaks ascribed to W metal appear. In the Al 2s spectra, the Al_2O_3 peak is present as well as before etching. After etching for 870 s, the peaks for the W metal become more intense relative to those of the W oxides, while the Al signal disappears.

The peak shifts in the W 4f spectra upon etching may imply that W in the metallic state is electrodeposited but the surface of the deposit is oxidized in air after electrodeposition. However, the electrodeposition of W metal cannot be concluded, because long-time Ar^+ etching during XPS measurement can reduce W oxides to a lower oxidation state, and eventually to W metal.[27] Whereas the oxidation state of W is ambiguous, Al clearly exists only in the oxide state, because Al 2s spectra do not show any peak shift after etching. The Al 2s signal disappears after the 870-s etching, while the W 4f signal is still clearly observed. This means that Al exists only in the vicinity of the deposited surface. Therefore, the Al_2O_3 detected by XPS is probably derived from residues of the bath components on the deposited surface. The large scattering of the W content determined by EDX (Fig. 3) is attributable to variations in the amount of residue from the bath components.

The examination of the deposits described above shows that Al-W alloy films containing up to 12 at.% W are electrodeposited at potentials <0 V, while deposits with a high content of W, whose oxidation state is unclear, are obtained at potentials >0 V.

Partial current density and current efficiency.—The amount of W in deposits obtained at each potential was measured with ICP-AES to calculate the partial current density for W deposition (J_W). The partial current density for Al deposition (J_{Al}) was also calculated from J_W and the W content of the deposits. The steady-state total current density (J_{total}), J_W, and J_{Al} are plotted against the deposition potential in Fig. 7. At potentials more positive than 0 V, J_W is calculated to be as low as 5.0×10^{-3} mA cm^{-2}, assuming that all the W atoms in the deposits are in the metallic state. As revealed by XPS, Al is not electrodeposited at potentials >0 V, and therefore J_{Al} is negligible.

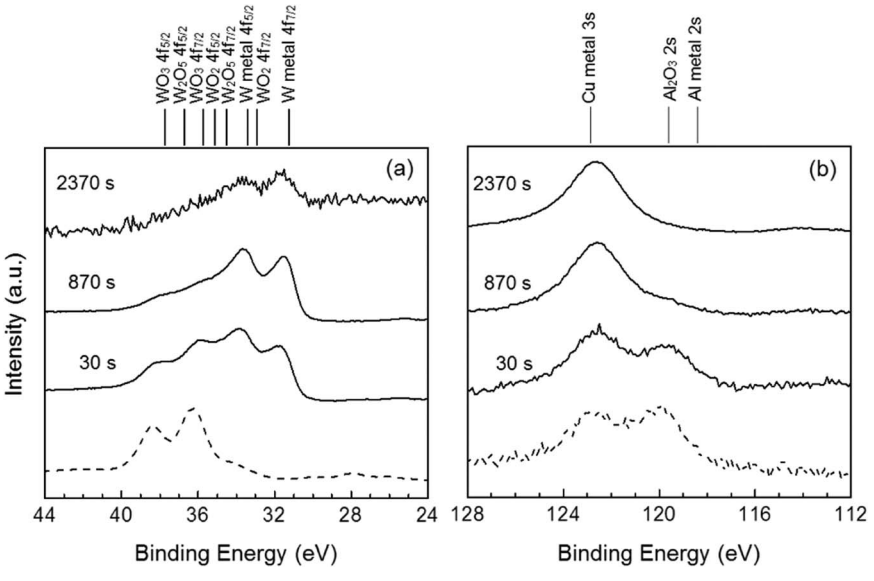

Figure 6. The XPS spectra of the deposit with 92 at.% W obtained at +0.3 V before (dashed line) and after (solid line) Ar^+ etching. The spectra are (a) W 4f, and (b) Al 2s. The etching times were 30, 870, and 2370 s. The binding energy of W metal, WO_2, W_2O_5, WO_3,[31] Al metal,[32] and Al_2O_3[33] are denoted at the top of the figure.

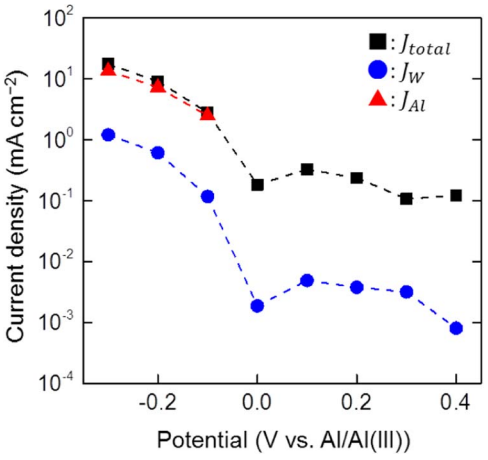

Figure 7. Steady-state total current density (J_{tatol}) and partial current densities for W and Al deposition (J_W and J_{Al}) during electrodeposition in an EMIC-2AlCl$_3$ bath containing 49 mM W_6Cl_{12}.

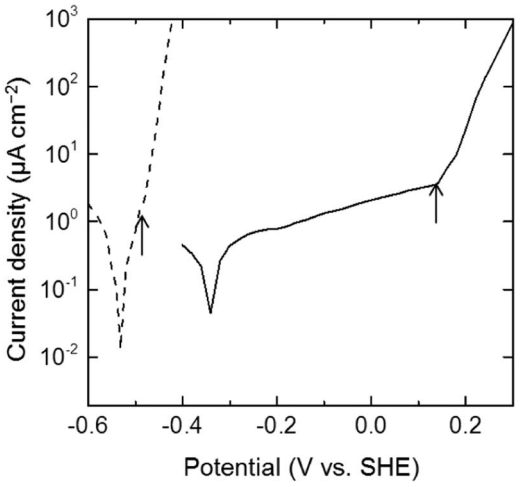

Figure 8. Polarization curves for the Al-W alloy film containing 10.5 at.% W (solid line) and an Al plate (dashed line) in 3.5 wt% aqueous NaCl solution. The scan rate was 0.5 mV s^{-1}. The pitting potential for each curve is indicated by the arrow.

From the comparison of J_W with J_{total}, the current efficiency for W deposition at potentials >0 V is estimated to be less than 2%. The current loss is most probably due to the reduction of protonic impurities in the electrolytic bath. The presence of protonic impurities was confirmed by a cathodic wave at around +1.0 V in cyclic voltammetry using a Pt electrode.[28] The deposition rate at potentials >0 V is so low that the impurity reduction current accounts for a large part of J_{total}, leading to the low current efficiency. Since the deposit is fragile as evidenced by the SEM image (Fig. 4a), exfoliation of the deposits from the electrode during electrodeposition could also be responsible for the low current efficiency. In contrast, at potentials <0 V, J_W as well as J_{Al} increase at more negative potentials and J_W reaches 1.2 mA cm^{-2} at −0.3 V. From the comparison of $J_W + J_{Al}$ with J_{total}, the current efficiency for Al-W alloy deposition is estimated to be approximately 90%.

The deposition rate is low at potentials >0 V, whereas the rate increases drastically when W is co-deposited with Al at potentials <0 V. This means that at potentials more negative than 0 V, the deposition of W is induced by the deposition of Al. This induced-electrodeposition behavior for W was not observed in the previous study on Al-W electrodeposition using $K_3W_2Cl_9$ as the W ion source. The difference in the deposition behaviors for W arises mainly from the solubility of the W ion source in the ionic liquid. Because the solubility of $K_3W_2Cl_9$ is low, the deposition rate of W is limited by the diffusion of W ions in the bath. In contrast, W_6Cl_{12} dissolves in the ionic liquid at a higher concentration, and therefore the deposition rate of W is increased by Al deposition without being limited by diffusion of the W ions.

Pitting corrosion resistance of Al-W alloy films.—As mentioned above, potentiostatic electrodeposition at <0 V yields dense and adherent Al-W alloy films containing up to 12 at.% W. The corrosion resistance of the Al-W alloy films was examined by measuring the pitting potential in 3.5 wt% aqueous NaCl solution through potentiodynamic polarization. Figure 8 shows polarization curves for an Al-W alloy film (10.5 at.% W) and an Al plate. In the polarization curve for the pure Al plate, the anodic current density presents a steep rise at −0.48 V, which is close to the rest potential (−0.53 V vs. SHE). Conversely, in the polarization curve for the Al-W alloy film, the anodic current density presents a steep rise at +0.14 V, which is more positive than the rest potential (−0.34 V). The steep rise in the anodic current density is attributed to the pitting corrosion on the surface. The Al-W alloy film exhibits a pitting potential that is +0.62 V more positive than that for the pure Al plate.

In a previous report, an Al-2.3 at.% W alloy film electrodeposited from an EMIC-2AlCl$_3$-$K_3W_2Cl_9$ bath displayed a pitting potential that was +0.3 V more positive than that for pure Al.[12] As reported in a series of studies on sputtered Al-W alloys, Al-W alloys exhibit higher pitting potentials with increasing W content.[1,3,4,6–8] However, the Al-W alloys electrodeposited from the $K_3W_2Cl_9$ bath had powdery morphologies and were easily exfoliated from the substrate when the W content was >5 at.%, making it difficult to carry out polarization experiments. In contrast, the Al-W alloys electrodeposited from the W_6Cl_{12} bath in the present study are dense and adherent, even when the W content is >10 at.%. As a result, the alloy film obtained from the W_6Cl_{12} bath shows a higher pitting potential than those from the $K_3W_2Cl_9$ bath.

Mechanical properties of Al-W alloy films.—The hardness (H) and Young's modulus (E) of the amorphous Al-W alloy film with 12.4 at.% W were determined by nano-indentation. An Al film electrodeposited from a bath containing no W_6Cl_{12} was also examined for comparison. Table I shows the H and E values of the Al-W alloy and Al films determined in this study, together with the values for Al and W bulk materials, which were extracted from the nano-indentation study reported in Oliver and Pharr (1992)[29] The Al film exhibits higher H and E values than those of the Al bulk material, because the former is composed of smaller grains and should have a residual stress. The H value of the Al-W alloy film is significantly higher than that of the pure Al film, and is close to that of the W bulk material. In contrast, the E value of the Al-W alloy film is close to that of the pure Al film, and is lower than that of the W bulk material. In general, crystalline metals which exhibit high H values also exhibit high E values. Contrary to this general trend, the Al-W alloy film with 12.4 at.% W exhibits high H and low E values, owing to its amorphous structure. In general, with no long-range atomic order, amorphous alloys exhibit high resistance to plastic deformation, thereby showing high hardness. In addition, amorphous alloys are less dense and have

Table I. Hardnesses (H) and Young's moduli (E) of an Al-W alloy film containing 12.4 at.% W, an electrodeposited Al film, and Al and W bulk materials. The values for Al and W bulk materials were extracted from Oliver and Pharr (1992).

Material	H (GPa)	E (GPa)
Al–12.4 at.% W film	4.6	89
Al film	1.7	97
Al bulk	0.3	68
W bulk	5.0	410

slightly larger interatomic spacing than their crystalline counterparts, allowing local atomic displacements that lead to stress relaxation. As a result, amorphous alloys exhibit stronger elastic behavior, leading to lower E values.[30] The high H and low E values of the amorphous Al-W alloy film are explainable by the same mechanism.

Conclusions

W_6Cl_{12} dissolves in an EMIC-2$AlCl_3$ ionic liquid at concentrations as high as 49 mM at 80°C. Potentiostatic electrodeposition at various potentials in the bath containing 49 mM W_6Cl_{12} revealed that Al-W alloy films containing up to 12 at.% W were electrodeposited at potentials more negative than 0 V vs. Al/Al(III). The deposition current density at >0 V was lower than 0.3 mA cm^{-2}, while that for Al-W alloy films was higher and reached 38 mA cm^{-2} at −0.5 V. The deposition of W was induced by the deposition of Al at potentials more negative than 0 V. The Al-W alloy films were composed of a super-saturated solid solution at lower W content, and they comprised an amorphous phase in the W content range of 9–12 at.%. The Al-W alloy films comprising an amorphous phase exhibited a high pitting corrosion resistance, high hardness, and low Young's modulus.

Acknowledgments

We thank Professor T. Doi (Kyoto University) for the SEM and EDX, Dr. Y. Sonobayashi (Kyoto University) for the XPS and Dr. R. Kasada (Kyoto University) for the nano-indentation. This work was supported by JSPS KAKENHI grant Number 25630327.

References

1. B. A. Shaw, T. L. Fritz, G. D. Davis, and W. C. Moshier, *J. Electrochem. Soc.*, **137**, 1317 (1990).
2. S. V. N. Naidu and P. R. Rao, Eds., *Phase Diagrams of Binary Tungsten Alloys*, Indian Institute of metals, Calcutta, (1991).
3. B. A. Shaw, G. D. Davis, T. L. Fritz, B. J. Rees, and W. C. Moshier, *J. Electrochem. Soc.*, **138**, 3288 (1991).
4. G. D. Davis, B. A. Shaw, B. J. Rees, and M. Ferry, *J. Electrochem. Soc.*, **140**, 951 (1993).
5. N. Radić, A. Tonejc, M. Milun, P. Pervan, J. Ivkov, and M. Stubičar, *Thin Solid Films*, **317**, 96 (1998).
6. M. Metikos-Hukovic, N. Radic, Z. Grubac, and A. Tonejc, *Electrochim. Acta*, **47**, 2387 (2002).
7. D. K. Merl, P. Panjan, and J. Kovač, *Corros. Sci.*, **69**, 359 (2013).
8. D. K. Merl, P. Panjan, and I. Milošev, *Surf. Eng.*, **29**, 281 (2013).
9. C. M. Rangel, M. A. Travassos, and J. Chevallier, *Surf. Coat. Technol.*, **89**, 101 (1997).
10. T. Tsuda, C. L. Hussey, and G. R. Stafford, *ECS Trans.*, **3**, 217 (2007).
11. T. Tsuda, Y. Ikeda, T. Arimura, A. Imanishi, S. Kuwabata, C. L. Hussey, and G. R. Stafford, *ECS Trans.*, **50**, 239 (2012).
12. T. Tsuda, Y. Ikeda, T. Arimura, M. Hirogaki, A. Imanishi, S. Kuwabata, G. R. Stafford, and C. L. Hussey, *J. Electrochem. Soc.*, **161**, D405 (2014).
13. W. R. Pitner, C. L. Hussey, and G. R. Stafford, *J. Electrochem. Soc.*, **143**, 130 (1996).
14. T. Tsuda, C. L. Hussey, G. R. Stafford, and J. E. Bonevich, *J. Electrochem. Soc.*, **150**, C234 (2003).
15. T. Tsuda and C. L. Hussey, *J. Min. Metall. B*, **39**(1–2), 3 (2003).
16. T. Tsuda, C. L. Hussey, G. R. Stafford, and O. Kongstein, *J. Electrochem. Soc.*, **151**, C447 (2004).
17. T. Tsuda, C. L. Hussey, and G. R. Stafford, *J. Electrochem. Soc.*, **151**, C379 (2004).
18. S. Ruan and C. A. Schuh, *Acta Mater.*, **57**, 3810 (2009).
19. T. Tsuda, S. Kuwabata, G. R. Stafford, and C. L. Hussey, *J. Solid State Electrochem.*, **17**, 409 (2013).
20. V. Kolesnichenko, D. C. Swenson, and L. Messerle, *Inorg. Chem.*, **37**, 3257 (1998).
21. M. Strobele, T. Justel, H. Bettentrup, and H.-J. Meyer, *Z. Anorg. Allg. Chem.*, **635**, 822 (2009).
22. S. Kamiguchi and T. Chihara, *Catal. Lett.*, **85**, 97 (2003).
23. G. Wilkinson, R. D. Gillard, and J. A. McCleverty, Eds., *Comprehensive Coordination Chemistry: The Synthesis, Reactions, Properties & Applications of Coordination Compounds*., Pergamon Press, Oxford, (1987).
24. W. C. Dorman and R. E. McCarley, *Inorg. Chem.*, **13**, 491 (1974).
25. P. A. Barnard, I. Sun, and C. L. Hussey, *Inorg. Chem.*, **29**, 3670 (1990).
26. A. N. Mansour, *Surf. Sci. Spectra*, **3**, 202 (1994).
27. H. Y. Wong, C. W. Ong, R. W. M. Kwok, K. W. Wong, S. P. Wong, and W. Y. Cheung, *Thin Solid Films*, **376**, 131 (2000).
28. S. Sahami and R. A. Osteryoung, *Anal. Chem.*, **55**, 1970 (1983).
29. W. C. Oliver and G. M. Pharr, *J. Mater. Res.*, **7**, 1564 (1992).
30. C. A. Schuh, T. C. Hufnagel, and U. Ramamurty, *Acta Mater.*, **55**, 4067 (2007).
31. A. Katrib, F. Hemming, P. Wehrer, L. Hilaire, and G. Maire, *J. Electron. Spectrosc. Relat. Phenom.*, **76**, 195 (1995).
32. C. Hinnen, D. Imbert, J. M. Siffre, and P. Marcus, *Appl. Surf. Sci.*, **78**, 219 (1994).
33. B. R. Strohmeier, *Surf. Sci. Spectra*, **3**, 141 (1994).